



Adsorption of gaseous ethylene via induced polarization on plasmonic photocatalyst Ag/AgCl/TiO₂ and subsequent photodegradation

Xizhuang Liang^a, Peng Wang^{a,*}, Mengmeng Li^b, Qianqian Zhang^a, Zeyan Wang^a, Ying Dai^b, Xiaoyang Zhang^a, Yuanyuan Liu^a, Myung-Hwan Whangbo^c, Baibiao Huang^{a,*}

^a State Key Laboratory of Crystal Materials, Shandong University, Jinan 250100, China

^b School of Physics, Shandong University, Jinan 250100, China

^c Department of Chemistry, North Carolina State University, Raleigh, NC 27695-8204, United States

ARTICLE INFO

Article history:

Received 7 May 2017

Received in revised form 20 July 2017

Accepted 25 July 2017

Available online 26 July 2017

Keywords:

Surface plasmon resonance (SPR)

Electric field

Induced polarization

Plasmonic photocatalyst

Nonpolar ethylene

ABSTRACT

The removal of nonpolar gaseous ethylene molecules on the plasmonic photocatalyst Ag/AgCl/TiO₂ was examined under simulated sunlight irradiation, to find that it has a markedly high activity for the oxidation of ethylene molecules. Systematic experiments, carried out to probe the cause for this observation, indicate that the strong electric field mainly on the Ag nanoparticles (NPs) generated by their surface plasmon resonance (SPR) induces polarization in gaseous ethylene molecules hence enhancing their adsorption on the catalysts and their subsequent photodegradation, and that TiO₂ acts as a substrate for dispersing Ag/AgCl nanoparticles to have a larger active surface area. This study provides new ideas towards designing advanced photocatalysts for the degradation of nonpolar gaseous molecules.

© 2017 Published by Elsevier B.V.

1. Introduction

It is a great challenge to effectively lower the activation energies for the reactions of small nonpolar molecules such as methane, ethylene and carbon dioxide because their nonpolar bonds have large bond dissociation energies [1–3]. Ethylene molecules help produce gaseous plant hormones, a small amount of which affects the growth, development and storage-life of many fruits and vegetables [4]. The harmful impact of ethylene on agricultural products during their transportation and storage is directly related to the concentration of ethylene around them [5,6]. Thus, it is an urgent problem to remove gaseous ethylene molecules during the transportation, storage and distribution. Due to the nonpolar nature and high bond dissociation energies of the C=C and C–H bonds, it is difficult to capture gaseous ethylene molecules on the surface of a catalyst and subsequently degrade it by photo-oxidation. Among several methods of removing ethylene [6–13], the photocatalytic oxidation is efficient and environmentally-friendly because it oxidizes ethylene to carbon dioxide and water at room or even subambient temperature [13].

NPs of noble metals Au and Ag exhibit a SPR phenomenon in the visible region due to the collective oscillations of their free electrons, which are triggered by the incident electromagnetic radiation [14]. The visible-light absorption induced by SPR can be tuned by changing the morphologies and sizes of the noble-metal NPs and their dielectric environments [15]. Over the past decade, except for the common construction of heterojunctions to increase the visible-light performance [16,17], the SPR phenomenon of noble-metal NPs has been employed in preparing numerous visible-light photocatalysts, which include M/TiO₂ (M = Au, Ag) [18–22], Au/ZnO [23], Ag/AgX (X = Cl, Br) [24–28] and Ag/AgCl/TiO₂ [29]. The photocatalysts Ag/AgX/TiO₂ (X = Cl, Br) have been extensively investigated for the removal of bacteria and hazardous pollutants in aqueous phase [29–32]. So far, however, there has been few reports on the decomposition of gaseous ethylene molecules using plasmonic photocatalysts.

Our theoretical study on Ag/AgCl showed [33] that the SPR of Ag NPs enhances the electric field in the plasmonic photocatalyst; the electric field at the interface of Ag NPs and AgCl substrate, mainly on the side of Ag NPs, is greatly increased. Due to their strong electric field, the Ag NPs of Ag/AgCl may induce polarization in small nonpolar gaseous molecules with polarizable electron cloud (e.g., those with π -electrons) and hence make it easy to adsorb them on the surface of Ag/AgCl and then photodegrade them. In this paper, we explore this possibility by studying the removal of

* Corresponding authors.

E-mail addresses: pengwangicm@sdu.edu.cn (P. Wang), bbhuang@sdu.edu.cn (B. Huang).

gaseous nonpolar ethylene $\text{CH}_2 = \text{CH}_2$ and gaseous polar vinyl chloride $\text{CH}_2 = \text{CHCl}$ using the plamsonic photocatalyst $\text{Ag}/\text{AgCl}/\text{TiO}_2$. We find that $\text{Ag}/\text{AgCl}/\text{TiO}_2$ has a markedly high activity for the oxidation of gaseous nonpolar ethylene molecules, and propose a plausible mechanism for this enhanced photoactivity.

2. Experimental sections

2.1. Materials and reagents

Tetrabutyl titanate (TBT), acetic acid (HAc), polyvinyl pyrrolidone (PVP), AgNO_3 , 1-octyl-3-methylimidazolium chloride ($[\text{C}8\text{Mim}]Cl$), ethanol and methanol were purchased from the Sinopharm Chemical Reagent Corporation (Shanghai, China). Commercial TiO_2 (P25) was purchased from Evonik. All chemicals were of analytical grade and were used without further purification.

2.2. Preparation of titania hierarchical microspheres (hereafter TiO_2)

The titania precursor hierarchical microspheres (TP-Hms) were synthesized using a hydrothermal process with TBT and HAc [34]. Typically, 3 ml TBT was dropwise added into 90 ml HAc with stirring for half an hour. After that, the solution was brought into 120 ml Teflon-lined stainless steel autoclave and maintained at 150 °C for 12 h. After cooling down to room temperature, the precipitates were washed with ethanol for several times, and finally dried in a vacuum oven at 70 °C for 6 h. The TP-Hms were calcined at several different temperatures for 2 h in air to obtain TiO_2 . Samples calcined at 500 °C for 2 h have better performance than those calcined at other temperatures, and will be referred to as TiO_2 -500.

2.3. Preparation of Ag/TiO_2 -500

The TiO_2 -500 (2.5 mmol) was added in 180 ml deionized water and 30 ml methanol under ultrasonic for 20 min. Then, 185 μl AgNO_3 solution (0.1 M) was dropped into the solution under magnetic stirring and continued to stir the suspension for another 30 min. All these processes were conducted in dark. Then, the solution was exposed to a 300 W Xenon lamp, and the color of the solution changed from white to brown after 30 min illumination. Finally, Ag/TiO_2 -500 samples were washed with water several times and dried in a vacuum oven at 60 °C for 6 h.

2.4. Preparation of $\text{Ag}/\text{AgCl}/\text{TiO}_2$

TiO_2 -500 (0.40 g), PVP and $[\text{C}8\text{Mim}]Cl$ were added in 90 ml deionized water and continually stirred for 1 h. Then AgNO_3 solution (0.1 M) was poured into the mixed solution, which was stirred continuously for about 30 min. The mixed suspension was transferred into a 120 ml Teflon-lined stainless steel autoclave, which was heated and maintained at 160 °C for 30 min and cooled down to room temperature. The product was washed several times with deionized water to remove any ionic residual and then dried in an oven at 60 °C for 6 h. AgCl/TiO_2 -500 samples with different Ag^+ concentrations were synthesized by adding 0.1 mmol ($\text{Ag}/\text{Ti} = 0.02$), 0.2 mmol ($\text{Ag}/\text{Ti} = 0.04$), 0.3 mmol ($\text{Ag}/\text{Ti} = 0.06$) and 0.4 mmol ($\text{Ag}/\text{Ti} = 0.08$) of AgNO_3 solution. Finally, the AgCl/TiO_2 samples were exposed to a 300 W Xenon lamp for 20 mins to get $\text{Ag}/\text{AgCl}/\text{TiO}_2$. The theoretical molar ratio ($\text{Ag}/\text{Ti} = 0.06$) in the samples shows the best performance than others, and will be referred to as $\text{Ag}/\text{AgCl}/\text{TiO}_2$ in the following.

2.5. Materials characterization

Powder X-ray diffraction (XRD) analyses were carried out with a Bruker AXS D8 advance powder diffractometer with Cu K α X-ray radiation. The scanning electron microscopy (SEM) images were obtained on a Hitachi S-4800 microscope with an Energy Dispersive Spectrometer (EDS). The detailed and clear nanostructure was characterized by transmission electron microscope (TEM, JEOL JEM-2100F). The photoluminescence (PL) measurements were carried out on a Hitachi F-4500 fluorescence spectrophotometer at room temperature with excitation wavelength at 320 nm. The nitrogen adsorption/desorption isotherm of samples was measured by a Kubo-X1000 apparatus. UV-vis diffuse reflectance spectroscopy (DRS) measurements were carried out with wavelength in the range of 800–200 nm on a Shimadzu UV 2550 recording spectrophotometer equipped with an integrating sphere. BaSO_4 was used as a reflectance standard.

2.6. Photocatalytic experiments

Photocatalytic degradation was carried out in a columnar quartz reactor with a total volume of 400 ml under light irradiation by a 300 W Xenon lamp or UV lamp (185 nm + 254 nm). First, for the degradation of ethylene C_2H_4 (vinyl chloride $\text{C}_2\text{H}_3\text{Cl}$), 0.3 g (0.05 g) samples were sprinkled uniformly at the bottom of the reactor. Second, 2 ml C_2H_4 or 2 ml $\text{C}_2\text{H}_3\text{Cl}$ were injected into the sealed quartz reactor by a micro-syringe. Third, the adsorption/desorption equilibrium of gas on the samples was obtained under magnetic stirring after 2 h in the dark. The reaction temperature of ethylene or vinyl chloride in the reactor was maintained at 5 °C by a water-cooling system. Finally, the system was exposed to a 300 W Xenon lamp or UV lamp (185 nm + 254 nm). At a certain time interval, 30 μl gas was withdrawn from the reactor. Simultaneous determination of ethylene or vinyl chloride concentrations were performed with an online gas chromatograph (Shimadzu GC-2014C and GCMS-QP2010 Ultra) equipped with a thermal conductivity detector (TCD) and a flame ionization detector (FID). The degradation percentage of gas was reported in terms of C/C_0 , where C is the concentration of the gas at a certain sampling time, and C_0 is the initial concentration of the gas injected.

2.7. Theoretical calculation

The density function theory (DFT) calculations were performed in VASP code [35], based on projector-augmented wave method (PAW) within the generalized gradient approximation (GGA) functional of Perdew-Burke-Ernzerhof (PBE) [36,37]. The 2×2 , 2×2 and 1×2 periodic slab models with 4, 4 and 9 layers atoms were constructed to model the Ag (001), AgCl (001) and TiO_2 (101) surface, respectively. 16 Å vacuum space was used to avoid the interaction between slabs. For all the slab models, the bottom two (for Ag and AgCl) or three atomic layers (for TiO_2) were frozen to the corresponding bulk structures, while the remaining layers were fully optimized until the force less than 0.02 eV/Å. The $3 \times 3 \times 1$ ($4 \times 4 \times 1$), $2 \times 2 \times 1$ ($3 \times 3 \times 1$) and $2 \times 3 \times 1$ ($3 \times 4 \times 1$) k-point meshes were adopted to sample the Brillouin zone of Ag , AgCl and TiO_2 surfaces for structure optimization (energy calculation). The 400 eV cutoff was applied for plane-wave basis set and the self-consistent field iteration was converged to 10^{-4} eV. The adsorption energy (E_{ads}) of ethylene on different surfaces was calculated as

$$E_{\text{ads}} = E[\text{slab} + \text{ethylene}] - E[\text{slab}] - E[\text{ethylene}] \quad (1)$$

where $E[\text{slab} + \text{ethylene}]$, $E[\text{slab}]$ and $E[\text{ethylene}]$ are the energies of ethylene adsorbed on surface, clean surface and free ethylene molecule, respectively. The polarization of ethylene was modeled by applying electric field along the C=C bond direction. Electron

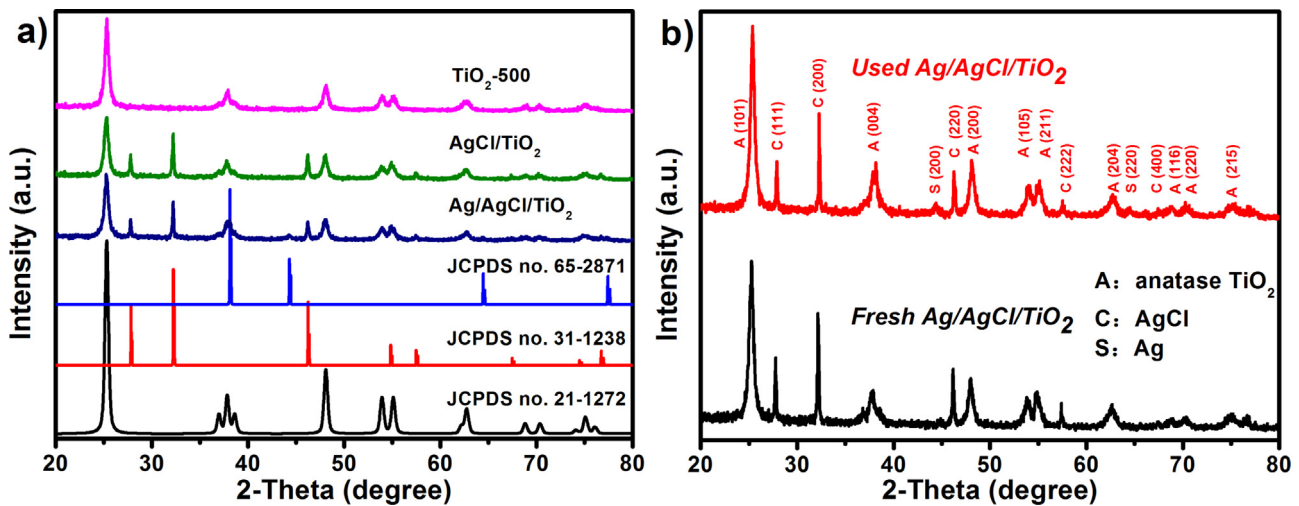


Fig. 1. XRD patterns: (a) As-prepared TiO₂-500, AgCl/TiO₂ and Ag/AgCl/TiO₂. (b) As-prepared fresh Ag/AgCl/TiO₂ and used Ag/AgCl/TiO₂ after four consecutive cyclic degradations of ethylene under (UV-vis) light illumination.

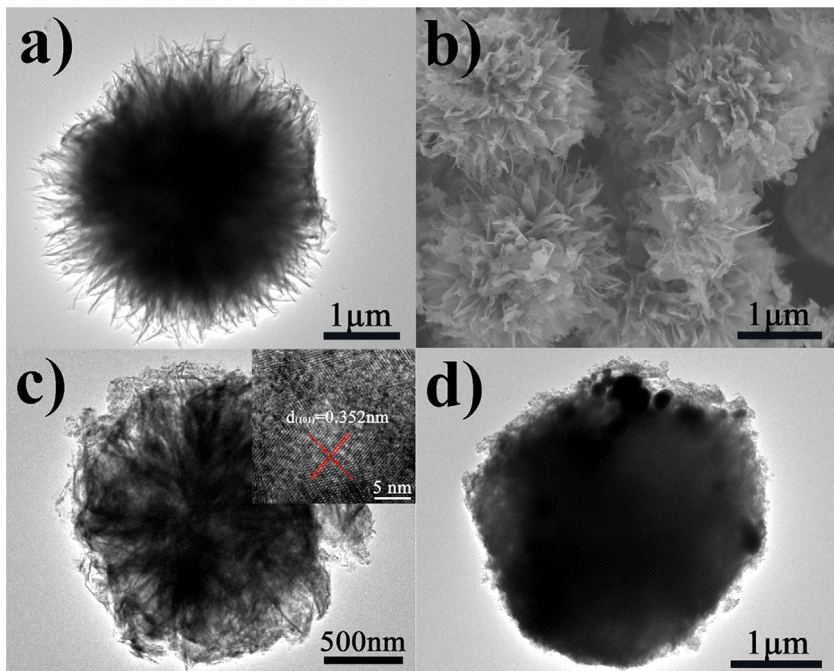


Fig. 2. (a) TEM image of TP-Hms. (b) SEM image of TiO₂-500. (c) TEM image of TiO₂-500 with HRTEM image in the inset. (d) TEM image of Ag/AgCl/TiO₂.

local function (ELF) was obtained by saving the ELFCAR output during statistic calculations.

3. Results and discussion

The XRD patterns of the as-prepared TiO₂-500, AgCl/TiO₂ and Ag/AgCl/TiO₂ are shown in Figs. 1 and S1. The characteristic diffraction peaks at 25.3°, 37.8°, 48.1°, 53.9° and 55.1° are attributed to (101), (004), (200), (105) and (211) crystal planes of anatase TiO₂ (JCPDS no. 21-1272). As for AgCl/TiO₂, the four diffraction peaks located at 27.8°, 32.2°, 46.2° and 57.5° are assigned to cubic AgCl (JCPDS no. 31-1238), which are indexed to the (111), (200), (220) and (222) crystal planes, respectively. These results indicate that both AgCl/TiO₂ and fresh Ag/AgCl/TiO₂ samples include anatase TiO₂ and cubic AgCl. In Fig. 1b, the peaks belonging to the anatase phase of TiO₂, the cubic phase of AgCl and the metallic Ag, are labeled with the letters A, C and S, respectively. Compared with

fresh Ag/AgCl/TiO₂, the XRD pattern of Ag/AgCl/TiO₂ used for four consecutive cyclic degradation of ethylene is similar to that of fresh Ag/AgCl/TiO₂, indicating the AgCl is stable during the degradation of ethylene. A few weak peaks, located at 44.3° and 64.4°, are assigned to metallic Ag (JCPDS no. 65-2871), indicating that some Ag NPs were produced by photoreducing some Ag⁺ ions on the surface of AgCl.

The TEM image of Fig. 2a shows that the TP-Hms consisting of long nanoribbons have an average diameter of around 3.0 μm. The SEM and TEM images (Fig. 2b and c) clearly reveal that the building units of TiO₂-500 changed from longer strips to wider nanosheets and NPs due to the decomposition of TP-Hms to TiO₂, CO₂ and H₂O. This is consistent with the previous report [34]. The calcination temperature displays no effect on the morphology of TiO₂, except for the small changes in the diameter of the spheres (Fig. S2). The high-resolution TEM (HRTEM) (inset in Fig. 2c) image demonstrates that the distinct lattice fringe of $d = 0.352\text{ nm}$ matches with

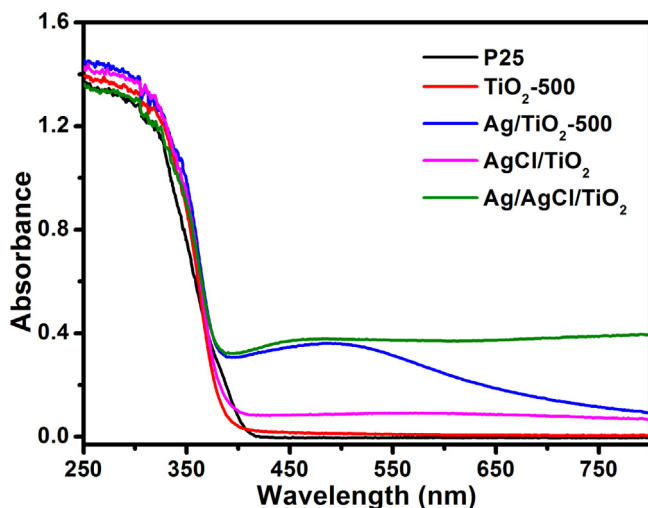


Fig. 3. UV-vis absorption spectra of P25, the TiO₂-500, Ag/TiO₂-500, AgCl/TiO₂, and Ag/AgCl/TiO₂.

the (101) crystallographic plane of anatase TiO₂, in good agreement with the XRD pattern (Fig. 1). It is generally difficult to distinguish Ag/AgCl from other NPs by TEM because AgCl is easily decomposed and converted to metallic Ag under high-energy electron or light beam. Nevertheless, the TEM image of Fig. 2d shows that Ag nanospheres with size from 50 to 100 nm near the surface of Ag/AgCl/TiO₂. The shape and size distribution of Ag NPs on the surface of the AgCl and TiO₂ vary over a large range. As a result, the SPR of the Ag NPs does not occur at a certain wavelength but spans a wide range of wavelength, permitting Ag/AgCl/TiO₂ to absorb visible and UV light over a wide range (see the DRS spectra below) [14,30]. In addition, the energy dispersive X-ray spectroscopy (EDX) measurement has also been carried out to identify the elemental compositions in Ag/AgCl/TiO₂ (Fig. S3 and Table S1).

The DRS spectra of P25 and the as-prepared photocatalysts are shown in Fig. 3. It is clear that P25 and TiO₂-500 display only UV absorption, with an absorption onsets of 400 nm and 385 nm, respectively. No obvious shift of the absorption edge can be observed for AgCl/TiO₂. After 1 wt% Ag NPs are deposited on the surface of TiO₂-500, a new broad absorption peak appears in the visible light region (430–550 nm), which is a characteristic SPR absorption of Ag NPs. [23,38,39]. Ag/AgCl/TiO₂ has strong absorption in the UV and visible-light regions (Fig. 3). Compared with AgCl/TiO₂, Ag/AgCl/TiO₂ exhibits a remarkable increase in the visible light absorption, which can be attributed to the SPR absorption of Ag NPs. The as-prepared plasmonic photocatalyst Ag/AgCl/TiO₂ absorbs in a wide region of the visible light because the TiO₂ substrate with a larger active surface area (Fig. S4 and Table S2) disperses Ag/AgCl NPs so that the Ag NPs have different sizes, shapes and environments. For another important role of the TiO₂ substrate in the photocatalytic activity of Ag/AgCl/TiO₂, see below.

Fig. 4 shows the PL spectra of TiO₂-500, AgCl/TiO₂ and Ag/AgCl/TiO₂, performed under the excitation wavelength of 320 nm. The emission spectra were recorded in the range of 340–600 nm and the emission peaks of both samples are similar, but the emission intensities are different. Generally, the lower PL intensity indicates the lower recombination rate of photogenerated electron-hole pairs and the higher photocatalytic activity of semiconductor photocatalyst. The intensity of PL spectra of Ag/AgCl/TiO₂ decreases significantly compared with TiO₂-500 and AgCl/TiO₂, indicating that introduction of Ag NPs suppressed the recombination of electrons and holes.

The photocatalytic activities of P25, TiO₂-500, Ag/TiO₂-500 and Ag/AgCl/TiO₂ were presented in Fig. 5. To mimic the real environ-

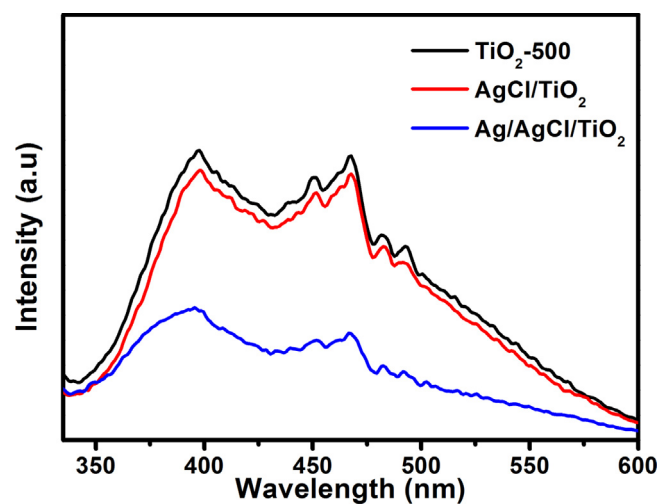


Fig. 4. PL spectra of TiO₂-500, AgCl/TiO₂ composite and Ag/AgCl/TiO₂ (with $\lambda_{\text{exc}} = 320 \text{ nm}$).

ment of fruit transportation, storage, and distribution, the reaction temperature was kept at 5 °C by a water-cooling system. Compared with P25, TiO₂-500 and Ag/TiO₂-500, Ag/AgCl/TiO₂ exhibits a dramatically improved activity for degrading ethylene under (UV-vis) light illumination (Fig. 5a). Ethylene is almost completely removed within 60 min over Ag/AgCl/TiO₂, while P25 displays only 40% degradation of ethylene within 60 min under the same reaction conditions. TiO₂-500 and Ag/TiO₂-500 exhibit nearly the same photodegradation activity as does P25. The degradation rate is about 4 times faster for Ag/AgCl/TiO₂ than for P25. To confirm that the degradation of ethylene is indeed caused by a photocatalytic process, we carried out control experiments, namely, one with catalysts but without light, and the other with the light but without catalysts. As shown in Fig. 5a and c, the control experiments show practically no degradation of ethylene, indicating that Ag/AgCl/TiO₂ is responsible for the photodegradation. In addition, calcination temperature is also investigated to find its effect on the photocatalytic activity. TiO₂-500 displays the best photocatalytic performance (Fig. S5a).

When the light of $\lambda > 420 \text{ nm}$ is cut off, the catalyst shows no activity for the degradation of ethylene. This might be due to the fact TiO₂ cannot be excited under visible light irradiation. Once the visible light is provided in addition to the specific UV wavelength, the activity of Ag/AgCl/TiO₂ for the ethylene oxidation is significantly improved (Fig. S5c). Under only UV light illumination, various photocatalysts display remarkably decreased activity, namely, the ethylene concentration decrease is 40% for P25, 36% for TiO₂-500, 24% for Ag/TiO₂-500, and 30% for Ag/AgCl/TiO₂ under the same reaction conditions (Fig. 5b). From the results obtained under irradiation of full arc light and only UV light, it is clear that the SPR of Ag NPs plays a vital role in the photodegradation of ethylene. As already mentioned, the SPR of the Ag NPs enhances the electric field at their interface with the AgCl substrate, mainly located on Ag nanoparticles. The latter can polarize ethylene molecules that are in the vicinity of the catalyst surface, making them adsorbed and resulting in a high probability for their degradation. P25 and TiO₂-500 cannot provide such effects because they have no strong electric field. Our previous studies [33,40] showed that the Ag NPs in Ag/AgCl have a wide range of diameters, and exist on the surface as well as in the inside of AgCl. Consequently, the Ag NPs have a wider range of SPR frequencies in Ag/AgCl/TiO₂ than in Ag/TiO₂, so that ethylene molecules have a higher probability of being polarized and subsequently absorbed on the surface of Ag/AgCl/TiO₂. To gain insight into the induced polarization fur-

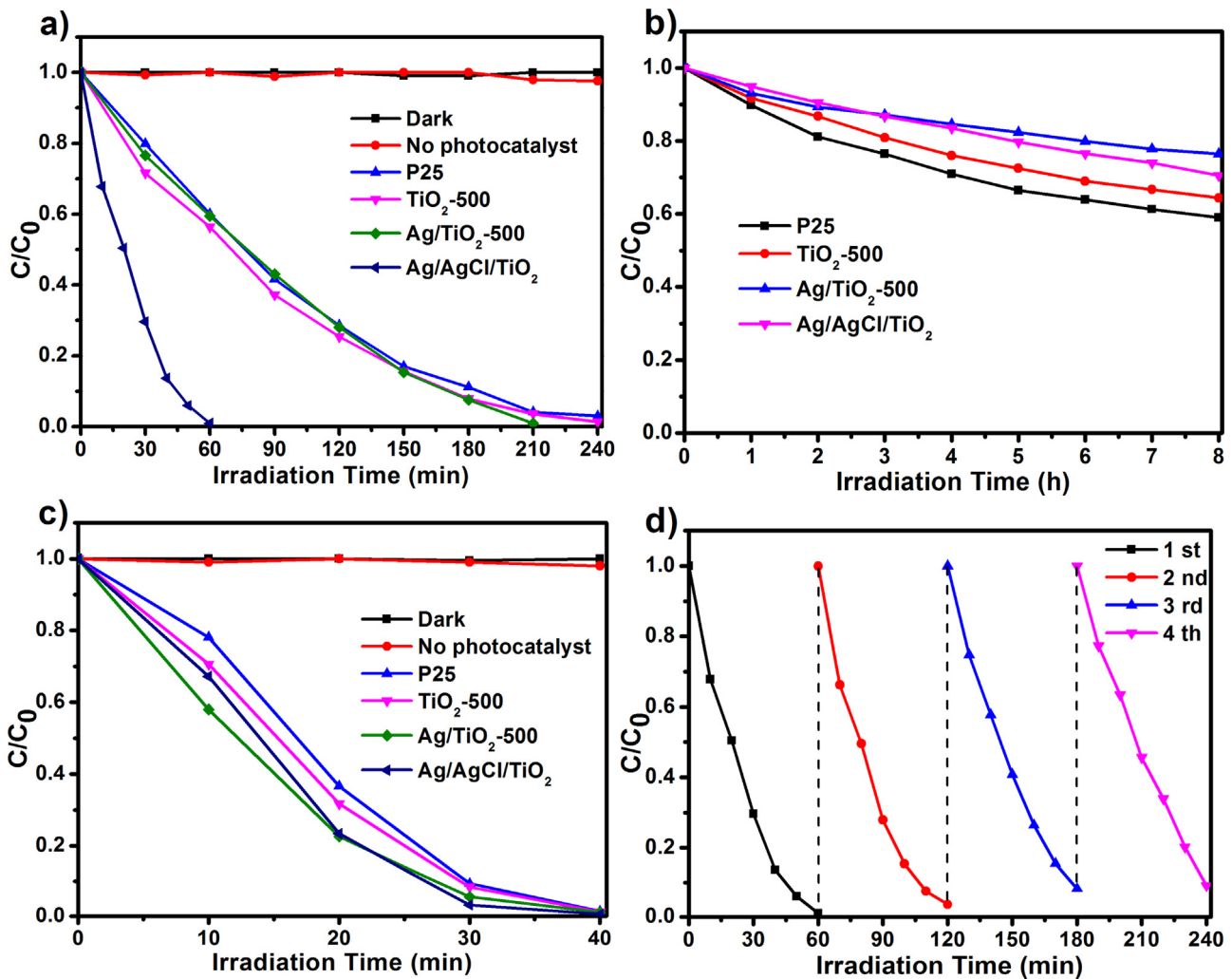


Fig. 5. (a) Photocatalytic degradation of ethylene in dark and under (UV-vis) light illumination using no photocatalyst, P25, TiO₂-500, Ag/TiO₂-500, and Ag/AgCl/TiO₂. (b) Photocatalytic degradation of ethylene under UV light illumination (185 nm + 254 nm) using P25, TiO₂-500, Ag/TiO₂-500, and Ag/AgCl/TiO₂. (c) Photocatalytic degradation of vinyl chloride in dark and under (UV-vis) light illumination using no photocatalyst, P25, TiO₂-500, Ag/TiO₂-500, and Ag/AgCl/TiO₂. (d) Four consecutive-cycle tests of the photocatalytic activity of Ag/AgCl/TiO₂ for ethylene degradation under (UV-vis) light illumination.

ther, we examined the activities of several photocatalysts using vinyl chloride, the C=C bond of which is already polarized by Cl. P25, TiO₂-500, Ag/TiO₂-500 and Ag/AgCl/TiO₂ display almost the same photocatalytic activities in the removal of vinyl chloride (Fig. 5c), showing that the presence of permanent polarization in vinyl chloride is important for the photocatalytic process. These results imply that the introduction of polarization in gaseous nonpolar ethylene molecules, induced by the strong electric field of the Ag NPs, is crucial for their adsorption on the surface of Ag/AgCl/TiO₂ and subsequent photodegradation.

The recyclability of a prepared sample was investigated by consecutive degradation experiments under simulated solar light irradiation. As shown in Fig. 5d, the four consecutive-cycle tests exhibit that the sample does not show any significant loss of photocatalytic activity for the degradation of ethylene. This is consistent with the result of the XRD result (Fig. 1b).

To account for the above observations, we propose a model depicted in Fig. 6. Gaseous nonpolar ethylene molecules in the vicinity of Ag/AgCl/TiO₂ are polarized by the strong electric field of the Ag NPs [41], thereby making them easily adsorbed on the surface of the photocatalyst. To test if this suggestion is reasonable, we carried out several DFT calculations. The induced dipole moment of an ethylene molecule generated by an external electric field (applied along the C=C direction) increases with increasing the field

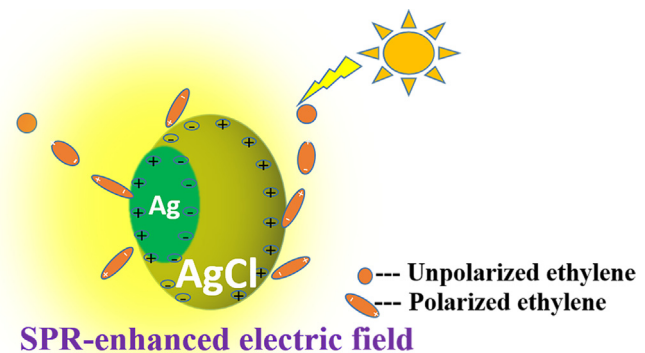


Fig. 6. Schematic diagram illustrating the adsorption of gaseous nonpolar ethylene. Ethylene molecules in the vicinity of the Ag NPs on the surface of Ag/AgCl/TiO₂ are polarized by their strong electric field and are subsequently adsorbed on the surface.

strength (Fig. S6 and Table S3). To investigate the influence of polarization on molecule adsorption on the main photocatalytic surfaces, we calculate the adsorption energies of unpolarized and polarized ethylene molecules on Ag, AgCl and TiO₂ surfaces. A slab model was used to simulate the Ag, AgCl or TiO₂ surface. To simulate polarized and unpolarized ethylene on the Ag, AgCl and TiO₂ surfaces, our

calculations for the ethylene on the Ag-, AgCl- or TiO₂-slab were carried out with and without an external field applied along the C=C bond direction. These calculations show that the adsorption energy of polarized ethylene molecules is lower compared with that of nonpolar ethylene (Table S4), and that the lowest adsorption energy of ethylene is obtained on AgCl surface for both the nonpolar and polarized molecule. Therefore, the experimental and theoretical results presented above suggest that the probable photocatalytic mechanism for the adsorption and degradation of gaseous ethylene on Ag/AgCl/TiO₂ is as follows: 1) When excited by visible light, the photocatalyst generates the SPR-enhanced electric field mainly on the side of Ag NPs. This polarizes nonpolar molecules in the vicinity of the catalyst (Fig. 6). 2) The polarized ethylene molecules are readily adsorbed on the surface of the plasmonic photocatalyst. 3) The adsorbed ethylene molecules are photo-degraded, most likely by trapping photogenerated electrons to become radicals, which further react with photogenerated holes to produce carbon dioxide and water.

4. Conclusion

In summary, in the Ag/AgCl/TiO₂ photocatalyst, the TiO₂ substrate disperses Ag/AgCl nanoparticles to have a larger active surface area and absorb in a wide region of the visible light. Furthermore, our work suggests that the TiO₂ substrate hinders the hole transfer to Cl⁻ to form Cl⁰ hence enhancing the hole transfer to O²⁻ to form O⁻. The Ag NPs increase the visible absorption due to the SPR, which generates a strong electric field largely on the Ag NPs. The latter induces polarization into nonpolar gaseous ethylene molecules that come in the vicinity of the catalyst, hence making them easily adsorbed on the Ag and AgCl surface sites and approach subsequently photodegraded. Our work presents a new to decomposing gaseous nonpolar molecules by plasmonic photocatalyst.

Acknowledgements

This work was financially supported by the National Basic Research Program of China (the 973 program, 2013CB632401), the National Natural Science Foundation of China (21333006, 21573135, 11374190, 51602179 and 51321091), P. Wang acknowledges support from The Recruitment Program of Global Experts, China. B.B.H. acknowledges support from the Taishan Scholars Program of Shandong Province.

Appendix A. Supplementary data

Supplementary data associated with this article can be found, in the online version, at <http://dx.doi.org/10.1016/j.apcatb.2017.07.075>.

References

- [1] W. Kutzelnigg, Angew. Chem. Int. Ed. 23 (1984) 272–295.
- [2] S.N. Pieniazek, F.R. Clemente, K.N. Houk, Angew. Chem. Int. Ed. 47 (2008) 7746–7749.
- [3] J.A. Labinger, J.E. Bercaw, Nature 417 (2002) 507–514.
- [4] M.E. Saltveit, Postharvest Biol. Technol. 15 (1999) 279–292.
- [5] A.A. Kader, HortScience 38 (2003) 1004–1008.
- [6] J.O. Kim, Process Biochem. 39 (2003) 447–453.
- [7] E.I. Papaioannou, S. Souentie, F.M. Sapountzi, A. Hammad, D. Labou, S. Brosda, C.G. Vayenas, J. Appl. Electrochem. 40 (2010) 1859–1865.
- [8] Q.H. Trinh, S.B. Lee, Y.S. Mok, J. Hazard. Mater. 285 (2015) 525–534.
- [9] G. Bailén, F. Guillén, S. Castillo, M. Serrano, D. Valero, D. Martínez-Romero, J. Agric. Food Chem. 54 (2006) 2229–2235.
- [10] K.L. Chang, K. Sekiguchi, Q.Y. Wang, F. Zhao, Aerosol Air Qual. Res. 13 (2013) 618–626.
- [11] D. Martínez-Romero, G. Bailén, M. Serrano, F. Guillén, J.M. Valverde, P. Zapata, D. Valero, Crit. Rev. Food Sci. Nutr. 47 (2007) 543–560.
- [12] M. Hussain, S. Bensaid, F. Geobaldo, G. Saracco, N. Russo, Ind. Eng. Chem. Res. 50 (2010) 2536–2543.
- [13] N. Keller, M.N. Ducamp, D. Robert, V. Keller, Chem. Rev. 113 (2013) 5029–5070.
- [14] P.V. Kamat, J. Phys. Chem. B 106 (2002) 7729–7744.
- [15] S. Linic, P. Christopher, D.B. Ingram, Nat. Mater. 10 (2011) 911–921.
- [16] D. Chen, K. Wang, D. Xiang, R. Zong, W. Yao, Y. Zhu, Appl. Catal. B Environ. 147 (2014) 554–561.
- [17] D. Yue, D. Chen, Z. Wang, H. Ding, R. Zong, Y. Zhu, Phys. Chem. Chem. Phys. 16 (2014) 26314–26321.
- [18] Z.K. Zheng, B.B. Huang, X.Y. Qin, X.Y. Zhang, Y. Dai, J.Y. Wei, M.-H. Whangbo, J. Mater. Chem. 21 (2011) 9079–9087.
- [19] R. Sellappan, M.G. Nielsen, F. González-Posada, P.C. Vesborg, I. Chorkendorff, D. Chakarov, J. Catal. 307 (2013) 214–221.
- [20] I.M. Arabatzis, T. Stergiopoulos, M.C. Bernard, D. Labou, S.G. Neophytides, P. Falaras, Appl. Catal. B Environ. 42 (2003) 187–201.
- [21] I.M. Arabatzis, T. Stergiopoulos, D. Andreeva, S. Kitova, S.G. Neophytides, P. Falaras, J. Catal. 220 (2003) 127–135.
- [22] C. Han, V. Likodimos, J.A. Khan, M.N. Nadagouda, J. Andersen, P. Falaras, P. Rosales-Lombardi, D.D. Dionysiou, Environ. Sci. Pollut. Res. 21 (2014) 11781–11793.
- [23] R.B. Jiang, B.X. Li, C.H. Fang, J.F. Wang, Adv. Mater. 26 (2014) 5274–5309.
- [24] P. Wang, B.B. Huang, X.Y. Qin, X.Y. Zhang, Y. Dai, J.Y. Wei, M.-H. Whangbo, Angew. Chem. Int. Ed. 47 (2008) 7931–7933.
- [25] P. Wang, B.B. Huang, X.Y. Zhang, X.Y. Qin, H. Jin, Y. Dai, Z.Y. Wang, J.Y. Wei, J. Zhan, S.Y. Wang, J.P. Wang, M.-H. Whangbo, Chem. Eur. J. 15 (2009) 1821–1824.
- [26] P. Wang, B.B. Huang, Q.Q. Zhang, X.Y. Zhang, X.Y. Qin, Y. Dai, J. Zhan, J.X. Yu, H.X. Liu, Z.Z. Lou, Chem. Eur. J. 16 (2010) 10042–10047.
- [27] P. Wang, B.B. Huang, Y. Dai, M.-H. Whangbo, Phys. Chem. Chem. Phys. 14 (2012) 9813–9825.
- [28] C. An, S. Peng, Y. Sun, Adv. Mater. 22 (2010) 2570–2574.
- [29] J.G. Yu, G.P. Dai, B.B. Huang, J. Phys. Chem. C 113 (2009) 16394–16401.
- [30] J.F. Guo, B.W. Ma, A.Y. Yin, K.N. Fan, W.L. Dai, J. Hazard. Mater. 211 (2012) 77–82.
- [31] Y. Hou, X.Y. Li, Q.D. Zhao, G.H. Chen, C.L. Raston, Environ. Sci. Technol. 46 (2012) 4042–4050.
- [32] B.Z. Tian, R.F. Dong, J.M. Zhang, S.Y. Bao, F. Yang, J.L. Zhang, Appl. Catal. B Environ. 158 (2014) 76–84.
- [33] X.C. Ma, Y. Dai, Y. Lin, Z.Z. Lou, B.B. Huang, M.-H. Whangbo, J. Phys. Chem. C 118 (2014) 12133–12140.
- [34] J.Y. Liao, J.W. He, H.Y. Xu, D.B. Kuang, C.Y. Su, J. Mater. Chem. 22 (2012) 7910–7918.
- [35] G. Kresse, J. Furthmüller, Comput. Mater. Sci. 6 (1996) 15–50.
- [36] P.E. Blöchl, Phys. Rev. B 50 (1994) 17953.
- [37] J.P. Perdew, J.A. Chevary, S.H. Vosko, K.A. Jackson, M.R. Pederson, D.J. Singh, C. Fiolhais, Phys. Rev. B 46 (1992) 6671.
- [38] L.Q. Jing, W. Zhou, G.H. Tian, H.G. Fu, Chem. Soc. Rev. 42 (2013) 9509–9549.
- [39] J. Tian, Z.H. Zhao, A. Kumar, R.I. Boughton, H. Liu, Chem. Soc. Rev. 43 (2014) 6920–6937.
- [40] X.C. Ma, Y. Dai, M. Guo, Y.T. Zhu, B.B. Huang, Phys. Chem. Chem. Phys. 15 (2013) 8722–8731.
- [41] X.Z. Cao, T.Y. Song, X.Q. Wang, Inorganic Chemistry, Higher Education Press, Beijing, 1994, pp. 195–199.